

# Brightest *Fermi*-LAT Flares of PKS 1222+216: Implications on Emission and Acceleration Processes

Pankaj Kushwaha<sup>1</sup>, K. P. Singh<sup>1</sup>, Sunder Sahayanathan<sup>2</sup>

## ABSTRACT

We present a high time resolution study of the two brightest  $\gamma$ -ray outbursts from a blazar PKS 1222+216 observed by the *Fermi* Large Area Telescope (LAT) in 2010. The  $\gamma$ -ray light-curves obtained in four different energy bands: 0.1–3, 0.1–0.3, 0.3–1 and 1–3 GeV, with time bin of 6 hr, show asymmetric profiles with a similar rise time in all the bands but a rapid decline during the April flare and a gradual one during the June. The light-curves during the April flare show  $\sim 2$  days long plateau in 0.1–0.3 GeV emission, erratic variations in 0.3–1 GeV emission, and a daily recurring feature in 1–3 GeV emission until the rapid rise and decline within a day. The June flare shows a monotonic rise until the peak, followed by a gradual decline powered mainly by the multi-peak 0.1–0.3 GeV emission. The peak fluxes during both the flares are similar except in the 1–3 GeV band in April which is twice the corresponding flux during the June flare. Hardness ratios during the April flare indicate spectral hardening in the rising phase followed by softening during the decay. We attribute this behavior to the development of a shock associated with an increase in acceleration efficiency followed by its decay leading to spectral softening. The June flare suggests hardening during the rise followed by a complicated energy dependent behavior during the decay. Observed features during the June flare favor multiple emission regions while the overall flaring episode can be related to jet dynamics.

*Subject headings:* radiation mechanisms: non-thermal – galaxies: active – FSRQs: individual: PKS 1222+216 (4C +21.35) – galaxies: jets – X-rays: galaxies

## 1. INTRODUCTION

The rapid, complex, high amplitude and broadband (radio to  $\gamma$ -rays) variability is a defining characteristic of a class of radio-loud active galactic nuclei (AGN) called blazars. These observed properties are believed to be a result of relativistic motion of non-thermal plasma along the jet, oriented at small angles to the observer's line of sight (Urry & Padovani 1995). The erratic variability combined with the complexity of organizing simultaneous multi-band observations and limitations of modern telescopes to resolve the emitting region makes multi-band variability studies and correlations as important tools to infer the underlying physical processes and the environment of AGNs. A detailed and systematic study of temporal and

---

<sup>1</sup>Department of Astronomy & Astrophysics, Tata Institute of Fundamental Research, Mumbai, India; pankaj563@tifr.res.in

<sup>2</sup>Astrophysical Sciences Division, Bhabha Atomic Research Centre, Mumbai, India

spectral features in different energy bands can offer a potential diagnostic for understanding the radiation mechanisms and underlying physical processes (Kirk et al. 1998; Kusunose et al. 2000; Bhattacharyya et al. 2005). For  $\gamma$ -ray bright AGNs with good photon statistics, the broadband energy coverage and continuous operation of *Fermi*-LAT offer a unique opportunity to extract multi-waveband light-curves down to scanning timescale of  $\sim 3$  hours (see Vasileiou (2013) for more details), making such a study feasible at  $\gamma$ -ray energies.

The radiative output of high luminosity blazars, particularly the flat spectrum radio quasars (FSRQs) is mostly dominated by  $\gamma$ -ray emission in the GeV regime and beyond in some cases (Begelman et al. 2008). This emission is generally explained as a result of inverse Compton (IC) scattering of photons external to the jet by non-thermal electrons (Nalewajko et al. 2012; Sikora et al. 2013), commonly referred as external Compton (EC). Two sites— one at sub-parsec scales and another at parsec scales, have been suggested for dominant  $\gamma$ -ray emission/contribution (Agudo et al. 2013; Dotson et al. 2012). On sub-parsec scales ( $< 1$  pc),  $\gamma$ -ray emission is due to the EC scattering of photons from broad line region (BLR) and/or accretion-disk (Finke & Dermer 2010), while on parsec scales the EC scattering of infrared (IR) photons from the putative molecular/dusty torus can be dominant. The sub-parsec scenario has been very successful in explaining the observed SED and short time  $\gamma$ -ray variability of blazars until very recently. However, the latest radio and  $\gamma$ -ray correlation studies (Agudo et al. 2013; Fuhrmann et al. 2014) favor parsec scenario in most cases with further support from the detection of FSRQs at very high energies (VHE; MAGIC Collaboration et al. 2008; Wagner & H.E.S.S. Collaboration 2010; Aleksić et al. 2011). In the parsec scale scenario; however, particle acceleration, bulk velocity, and emission regions associated with short time variability of few minutes to hours are matters of ongoing debate due to its larger distance from the central engine (Nalewajko et al. 2012; Agudo et al. 2013; Kushwaha et al. 2014).

Most of the studies till date have relied on spectral features (Abdo et al. 2011; Tanaka et al. 2011) and constraints from  $\gamma$ -ray opacity to infer the underlying mechanisms, seed photons and hence the location of emission sites in blazars (Aleksić et al. 2011; Tanaka et al. 2011; Nalewajko et al. 2012; Sahayanathan & Godambe 2012; Kushwaha et al. 2014). However, spectral information from  $\gamma$ -ray emission is subject to Klein-Nishina (KN) softening, pair production and presence of intrinsic features in the particle spectra, making GeV emission and underlying processes hard to disentangle (Dotson et al. 2012). Moreover, if the underlying physical processes (particle acceleration and injection) are evolving faster than the cooling timescales, as suggested by the observations in cases of high luminosity blazars (Kushwaha et al. 2014), spectral information averaged over a longer duration data may lead to false inferences regarding these processes. High time resolution study of spectral, timing and variability features though, can be used to infer these timescales and their relative dominance, at least for bright sources. This, in fact, can also differentiate between multiple injections/emission-regions which on larger timescales seem coherent otherwise (Saito et al. 2013; Brown 2013). However, only a truly simultaneous multi-band study holds the key to gain further insight into these enigmatic processes (Kirk et al. 1998; Chiaberge & Ghisellini 1999).

PKS 1222+216 (4C +21.35<sup>1</sup>;  $z = 0.432$ ) is a lobe dominated FSRQ at long radio wavelengths (cm

---

<sup>1</sup>PKS 1222+21, PKS B1222+216

onwards) and a known  $\gamma$ -ray emitter (Tanaka et al. 2011; Ackermann et al. 2014, and references therein). In high resolution radio maps, it shows a strong jet bending (Saikia et al. 1993; Cooper et al. 2007) and superluminal knots with complex 3D trajectories suggesting non-radial accelerations (Homan 2012; Ackermann et al. 2014). Increased  $\gamma$ -ray activity from the source was reported by *Fermi*-LAT during April 2009 (Longo et al. 2009). Since December 2009 till mid 2010, it has been particularly active at  $\gamma$ -ray energies undergoing frequent and rapid flux variations (Ciprini 2009). Enhancements were also seen by other observatories operating at similar/different energy-bands (Verrecchia et al. 2009; Bulgarelli et al. 2010; Carrasco et al. 2010). During this period the source showed two prominent  $\gamma$ -ray flares ( $> 10^{-5} \text{ph cm}^{-2} \text{s}^{-1}$ ): one in April 2010 (Donato 2010) and another in June 2010 (Iafrate et al. 2010), the brightest so far in LAT band from this source<sup>2</sup>. A detailed investigation of LAT data during April flare confirmed VHE emission (129 GeV photon; Neronov et al. 2010, 2011) leading to the inclusion of PKS 1222+216 in the LAT VHE catalog (Neronov et al. 2011). During this high  $\gamma$ -ray activity period, two VHE excesses were detected by the *MAGIC* observatory– one immediately after the end of the April flare on MJD 55319.97 (Ackermann et al. 2014) and other one during the rising part of the June 2010 flare (Mose Mariotti 2010; Aleksić et al. 2011) establishing PKS 1222+216 as a potential VHE FSRQ.

First two years of *Fermi*-LAT observations of PKS 1222 + 216 have been analyzed by Tanaka et al. (2011) by dividing the LAT light-curve in different activity states based on the observed  $\gamma$ -ray variability of the source. They have further performed a detailed investigation of the LAT data for the time period considered in this paper (the *Active* state of Tanaka et al. (2011)), focusing particularly on the spectral evolution,  $\gamma$ -ray emission and energetics of the source during its different activity states. Based on the spectral fit of LAT spectral energy distribution (SED) and the stability of the break energy during its various activity states, the authors argued that the break can be well explained by recombination in the BLR as suggested by Poutanen & Stern (2010). However, EC scattering of BLR photons (Lyman- $\alpha$ ) to VHE lies in the KN regime, making VHE emission extremely inefficient with a significant emission only up to few 10s of GeV (Nalewajko et al. 2012; Kushwaha et al. 2014). Detection of VHE photons during both the prominent flares in 2010 and a hard VHE spectra during the June 2010 flare (Aleksić et al. 2011) contradict the BLR origin (Tavecchio et al. 2011; Sahayanathan & Godambe 2012; Nalewajko et al. 2012), though it can contribute significantly at GeV energies.

In this paper, we present a detailed systematic analysis of variability during the two brightest  $\gamma$ -ray flares of PKS 1222+216 mentioned above. The continuous broadband observation of *Fermi*-LAT and the strong fluence allowed us to extract  $\gamma$ -ray light-curves down to a timescale of 6 hours in four different LAT energy bands: 0.1–3 GeV, 0.1–0.3 GeV, 0.3–1 GeV and 1–3 GeV. Details of *Fermi*-LAT data and its reduction procedures are discussed in Section 2. In Section 3, we present the main results obtained from the LAT analysis, with its implications on blazar emission and underlying physical processes being discussed in Section 4. Finally we summarize our finding in Section 5. A standard  $\Lambda$ CDM cosmology has been assumed throughout this paper with  $\Omega_m = 0.3$ ,  $\Omega_\Lambda = 0.7$  and  $H_0 = 70 \text{ km s}^{-1} \text{ Mpc}^{-1}$ .

---

<sup>2</sup>[http://fermi.gsfc.nasa.gov/FTP/glast/data/lat/catalogs/asp/current/lightcurves/PKSB1222+216\\_86400.png](http://fermi.gsfc.nasa.gov/FTP/glast/data/lat/catalogs/asp/current/lightcurves/PKSB1222+216_86400.png)

## 2. DATA REDUCTION

The pair conversion detector known as Large Area Telescope (LAT) on board *Fermi Gamma-ray Space Telescope* is sensitive to  $\gamma$ -ray photons with energies 20 MeV to  $> 300$  GeV (Atwood et al. 2009). It operates mostly in survey mode scanning the entire sky every  $\sim 3$  hours, thereby offering a unique capability for studying short time evolution of  $\gamma$ -ray sources. Here, we have analyzed the LAT data of PKS 1222+216 from April-June 2010 (see Table 1) when it was undergoing intense  $\gamma$ -ray activity and had emitted two brightest GeV flares of intensity  $\gtrsim 10^{-5}$  ph cm $^{-2}$  s $^{-1}$  with  $\gamma$ -ray emission extending up to VHEs.

Table 1: Log of *Fermi*-LAT observations

Start Date (MJD)	End Date (MJD)	State
April 14, 2010 (55300)	June 27, 2010 (55375)	Active
April 27, 2010 (55313)	May 01, 2010 (55318)	<i>Flare 1</i>
June 16, 2010 (55363)	June 22, 2010 (55370)	<i>Flare 2</i>

LAT data studied here (see Table 1) were analyzed using *Fermi*-LAT Science tool version v9r27p1 following the recommended analysis procedure<sup>3</sup>. Only events classified as “evclass=2”, energy  $> 100$  MeV and zenith angles  $< 100^\circ$  from a region of interest (ROI) of  $15^\circ$  centered around the source were considered during our analysis to avoid calibration uncertainties and the earth’s limb. Good time intervals associated with the selected events were calculated using the recommended selection “(DATA\_QUAL==1)&&(LAT\_CONFIG==1)&&ABS(ROCK\_ANGLE)< 52”. Effects of various cuts on data and sources outside the ROI were taken into account by calculating exposure map on ROI and an additional annulus of  $10^\circ$  around ROI. The selected events were then analyzed using “unbinned maximum likelihood” method (Mattox et al. 1996, PYTHON implementation of *glike*). Sources within the angular field of exposure map were selected and modeled using 2nd LAT catalog (2FGL – gll\_psc\_v08.fit; Nolan et al. 2012) and the *Pass 7* instrument response function (*P7SOURCE\_V6*). Galactic diffuse emission and isotropic background were taken into account by using the respective template (gal\_2yearp7v6\_v0.fits, iso\_p7v6source.txt).

The daily 0.1–300 GeV LAT  $\gamma$ -ray light-curve during the entire episode was extracted following the above procedures and assuming a log-parabola model [ $dN/dE \sim E^{-\alpha-\beta \log(E)}$ ] for the source (Nolan et al. 2012). We have used a logarithmically equi-spaced, twenty energy grids, per energy decade for the spectral fit. Point sources with test statistic (TS)  $\leq 0$  (equivalent of standard deviation  $\sigma^2$ ) were removed from the source model files during each analysis. The 6 hr light-curves in four different LAT energy bands: 0.1 – 3 GeV, 0.1 – 0.3 GeV, 0.3 – 1 GeV and 1 – 3 GeV, during *Flare 1* and *Flare 2* were extracted using the best fit model files from the longer duration analysis as input model. A TS value of 10 ( $\sim 3\sigma$ ) was used as a detection criteria for the source. The systematic uncertainties associated with the derived fluxes are 10% at 0.1 GeV and 5% between 0.316 GeV to 10 GeV.

---

<sup>3</sup>[http://fermi.gsfc.nasa.gov/ssc/data/analysis/scitools/python\\_tutorial.html](http://fermi.gsfc.nasa.gov/ssc/data/analysis/scitools/python_tutorial.html)

### 3. ANALYSIS AND RESULTS

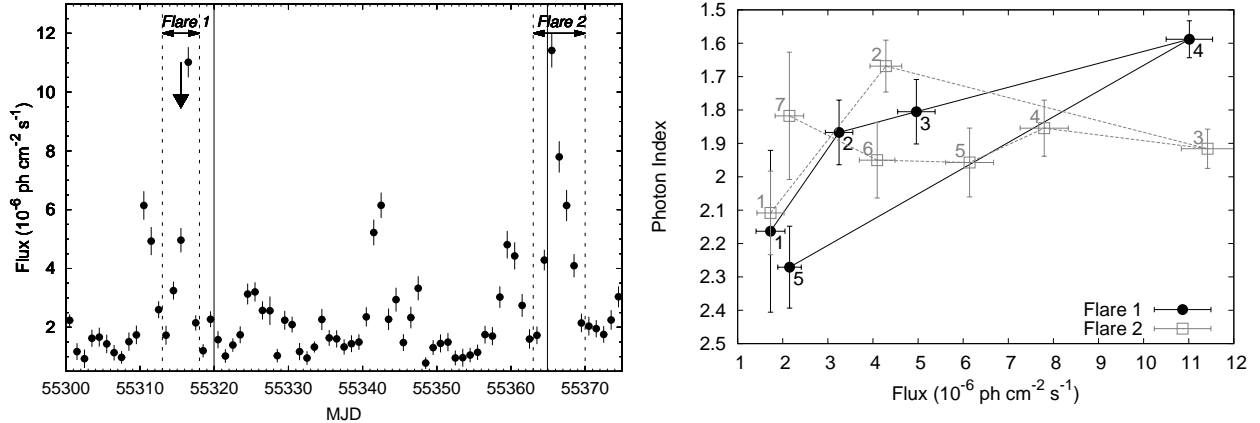


Fig. 1.— *Left*: The daily binned 0.1–300 GeV *Fermi*-LAT light-curve of PKS 1222+216 during its active period (see Table 1) in 2010. The dashed vertical lines mark the intervals of the two brightest  $\gamma$ -ray flares from PKS 1222+216 observed by the *Fermi*-LAT till date. The vertical solid lines and the black arrow indicate the epochs of detection of VHE emission by the *MAGIC* observatory and the *Fermi*-LAT respectively. Error bars represent statistical  $1\sigma$  limit. *Right*: Variation of spectral indices with observed fluxes during *Flare 1* (black solid line and filled circles) and *Flare 2* (grey dashed line and empty squares) marked by numbers indicating the day from the start of the respective flare.

The 0.1–300 GeV LAT  $\gamma$ -ray light-curve of the source extracted on a day timescale during the time interval analyzed here (see Table 1) is shown in the left panel of Figure 1. The period is characterized by a rapid and frequent flux variations at  $\gamma$ -ray energies, and five major flares of fluxes  $F > 4 \times 10^{-6}$  ph  $\text{cm}^{-2}$   $\text{s}^{-1}$  are observed. Two of these, recorded respectively in April and June 2010 have similar amplitudes ( $F \gtrsim 10^{-5}$  ph  $\text{cm}^{-2}$   $\text{s}^{-1}$ ). The two flares, marked by dotted lines with labels *Flare 1* and *Flare 2* respectively in the left panel of Fig. 1 are also the brightest  $\gamma$ -ray flares from this source in the history of *Fermi*-LAT operation till date. The right panel of Fig. 1 shows the daily variation of spectral index as a function of the observed flux (index-flux hysteresis) with numbers indicating the day from the onset of the respective flare. A clear clockwise (CW) evolution of index-flux hysteresis can be seen during both the flares. Interestingly, both the flares were preceded by a relatively smaller amplitude ( $\sim 0.5$  of *Flare 1* peak) and similar duration flares. Despite their similar flux, CW evolution of index-flux hysteresis, and the preceding history, both *Flare 1* and *Flare 2* reveal a characteristically different temporal patterns during the flaring episodes. The LAT flux during *Flare 1* reaches its peak in 4 days and falls rapidly within a day. On the contrary, *Flare 2* reaches its peak within 3 days and shows a gradual fall lasting 4 days. Gamma-ray emission extending up to VHE (*Flare 1*:  $\sim 130$  GeV, *Flare 2*:  $\sim 400$  GeV) was detected just before the LAT peak during both these flares. The vertical arrow in Fig. 1 (left panel) shows the time when VHE emission was detected in LAT during *Flare 1* (129 GeV, Neronov et al. 2010) while the solid line during *Flare 2* marks the VHE detection by the *MAGIC* observatory (Mose Mariotti 2010; Aleksić et al. 2011). Another  $4.4\sigma$  VHE detection has been claimed on MJD 55320 in the *MAGIC* data, and is shown by a vertical solid line in Fig. 1 during the

$\gamma$ -ray active period of the source (Ackermann et al. 2014).

### 3.1. Flux Variability

LAT  $\gamma$ -ray light-curves of PKS 1222+216 during *Flare 1* and *Flare 2* in four different energy bands: 0.1 – 3 GeV, 0.1 – 0.3 GeV, 0.3 – 1 GeV and 1 – 3 GeV at 6 hr timescale are shown respectively in the left and right panel of Figure 2. Except for the 1–3 GeV emission, both flares have similar peak fluxes in respective energy bands, but present a different case with respect to temporal features, variability and sub-structures.

To access the asymmetry of rise and decay of the flares, we have fitted an exponential rising and falling profile

$$f(t) = C + A(\exp[(t - t_p)/t_r] + \exp[-(t - t_p)/t_f])$$

where  $t_r$  and  $t_f$  are rise and fall time in days with C, A and  $t_p$  being a constant (quiescent flux), normalization (half of peak flux) and the instant of the flare peak respectively. First, the quiescent flux was derived by fitting a constant to a selected range of the 6 hr light-curve in each energy band. Fit was then performed on the 0.1 – 3 GeV light-curves restricting the quiescent flux (C) to vary within its best fit limits. The subsequent fitting in the other three energy bands was then performed by fixing the peak position to this best fit value. The results from the fits and associated  $1\sigma$  errors are given in Table 2. The fitted profiles, plotted only for data considered during the fitting, are shown in the left and right panel of Figure 2.

Table 2: Flare characteristics– Best fit values with  $1\sigma$  errors

Energy Band (GeV)	No. of time bins	C ( $10^{-6}$ ph cm $^{-2}$ s $^{-1}$ )	A	$t_0$ (MJD)	Rise time ( $t_r$ ) (days)	Fall time ( $t_f$ ) (days)	$\chi^2$ (dof)
<i>Flare 1</i>							
0.1–3.0	20	$1.5 \pm 0.2$	$16.8 \pm 0.2$	$55316.74 \pm 0.05$	$0.6 \pm 0.1$	$0.13 \pm 0.05$	30.9 (15)
0.1–0.3	16	$1.6 \pm 0.2$	$9.3 \pm 1.6$	–	$0.5 \pm 0.1$	$0.07 \pm 0.02$	9.5 (12)
0.3–1.0	18	$2.3 \pm 0.2$	$4.8 \pm 0.5$	–	$0.9 \pm 0.1$	$0.20 \pm 0.03$	19.7 (14)
1.0–3.0	11	$0.12 \pm 0.02$	$2.7 \pm 0.5$	–	$0.4 \pm 0.1$	$0.11 \pm 0.03$	11.3 (7)
<i>Flare 2</i>							
0.1–3.0	28	$1.8 \pm 0.2$	$11.8 \pm 0.8$	$55365.5 \pm 0.1$	$0.6 \pm 0.1$	$1.5 \pm 0.1$	49.2 (23)
0.1–0.3	28	$1.4 \pm 0.2$	$7.4 \pm 0.7$	–	$0.6 \pm 0.1$	$1.6 \pm 0.2$	34.4 (24)
0.3–1.0	26	$0.57 \pm 0.03$	$3.7 \pm 0.3$	–	$0.5 \pm 0.1$	$1.2 \pm 0.1$	15.2 (22)
1.0–3.0	27	$1.1 \pm 0.2$	$0.9 \pm 0.1$	–	$0.9 \pm 0.2$	$1.5 \pm 0.2$	21.5 (23)

### 3.2. Hardness Ratios

The left and right panel of Fig. 3 show the daily 0.1-300 GeV  $\gamma$ -ray light-curve along with the corresponding hardness ratios (HRs) during *Flare 1* and *Flare 2*. We have derived two hardness ratios, HR1 and

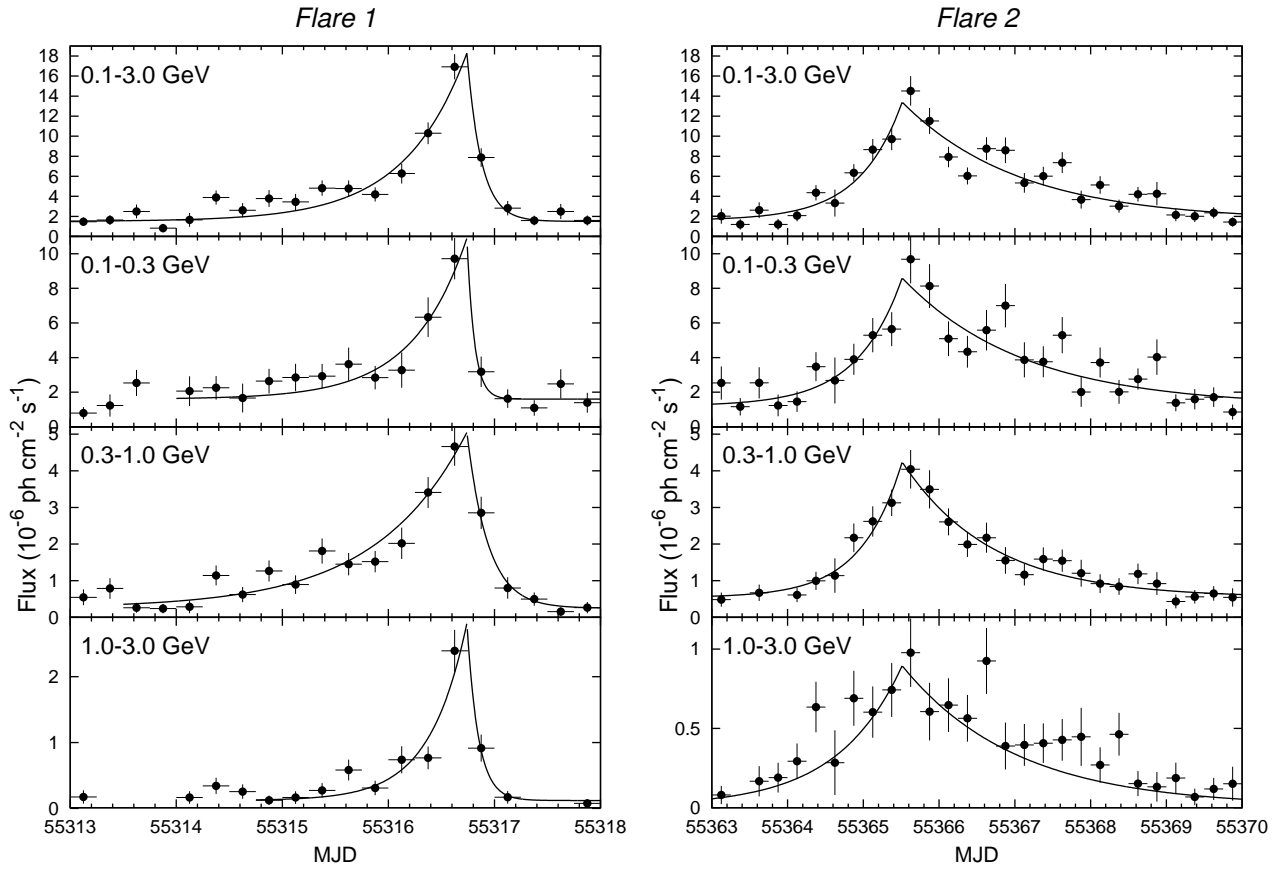


Fig. 2.— 6 hr  $\gamma$ -ray light-curves of PKS 1222+216 during *Flare 1* (left) and *Flare 2* (right) in four different LAT energy bands. The solid black curves are the best fit temporal profiles assuming an exponential rise and fall (see Table 2, §3.1).



HR2, defined as the ratio of flux in 0.3–1 GeV to the corresponding flux in the 0.1–0.3 GeV band, and the ratio of 1–3 GeV flux to the corresponding 0.3–1 GeV flux, respectively. Though the peak fluxes are similar, the hardness ratios show very different evolution during the rise, at the peak and during the decay phase of the flares. Both HR1 and HR2, during *Flare 1*, show a consistent hardening until the peak followed by a softening to quiescent level during the flare decay. HR1 and HR2 during *Flare 2*, on the other hand, suggest a hardening during the rising phase but a reverse trend at the peak and a different evolution behavior during the decay phase. HR1 at peak is consistent with hardening seen during the rising phase and softens during the decay but not to the quiescent level. HR2, on the contrary, softens to quiescent level at the peak and remains at the same level throughout the decay phase of *Flare 2*.

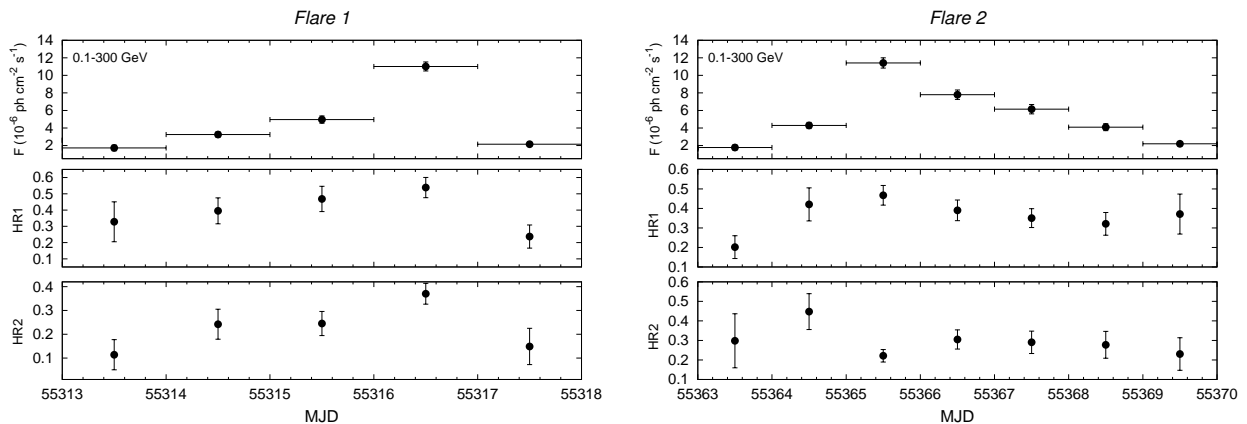


Fig. 3.— Variability of flux (0.1–300 GeV) and Hardness ratios (HR1, HR2) on daily time-scale during *Flare 1* and *Flare 2* (§3.2).

### 3.3. Time Delay/Lag

It is interesting to note that VHE photons (Neronov et al. 2010; Mose Mariotti 2010; Aleksić et al. 2011) precede the LAT peak during both the flaring episodes suggesting a soft lag<sup>4</sup>. In general, the origin of flares in BLR (torus) is expected to have absence (presence) of time lag between the MeV and GeV emission (Dotson et al. 2012). Motivated by this, we performed a lag analysis to look for a possible hint, if any, between the extracted LAT light-curves in different energy bands. The analysis is, however, limited by closely separated energy bands and best available time resolution of 6 hr. The lag analysis was performed using *z-transformed Discrete Correlation Function* (ZDCF) method of Alexander (2013) (also see Alexander (1997)). It works on data pairs sorted according to their time lag and binned into equal population bins of at least 11 pairs after discarding multiple occurrences of the same data pair in a bin. Correlation coefficients of the bins are calculated and then *z-transformed* to estimate the error in *z-space* which are then transformed back in the correlation space. DCF errors are estimated using Monte Carlo simulations by adding a ran-

<sup>4</sup>A clear peak in VHE was detected during *Flare 2* by the *MAGIC* observatory on  $\sim 55364.92$  but not during *Flare 1*



dom error at each step to each data from the errors in the light-curves fluxes (see Alexander 2013, for more details).

The time lag analysis was carried out on a continuous set of uniformly sampled data points during both the flares, though the method used is also applicable in the case of non-uniformly sampled light-curves<sup>5</sup>. The results of the lag analysis derived from 1000 simulations of each pair, and the associated  $1\sigma$  uncertainties are given in Table 3. The corresponding DCFs for *Flare 1* and *Flare 2* are presented in the left and right panel of Fig. 4 respectively where the time ordering is “T(2nd light-curve:LC2) – T(1st light-curve:LC1)”. Our analysis suggests a soft lag between the lowest and the highest energy light-curves during *Flare 2* while *Flare 1* is consistent with no lag. Considering the low significance of the inferred soft lag during *Flare 2*, it has to be understood as an upper-limit only. Further, there may be a lag among all the three light-curves but the limited time resolution provided by the LAT light-curves and the closeness of energy bands makes it hard to ascertain.

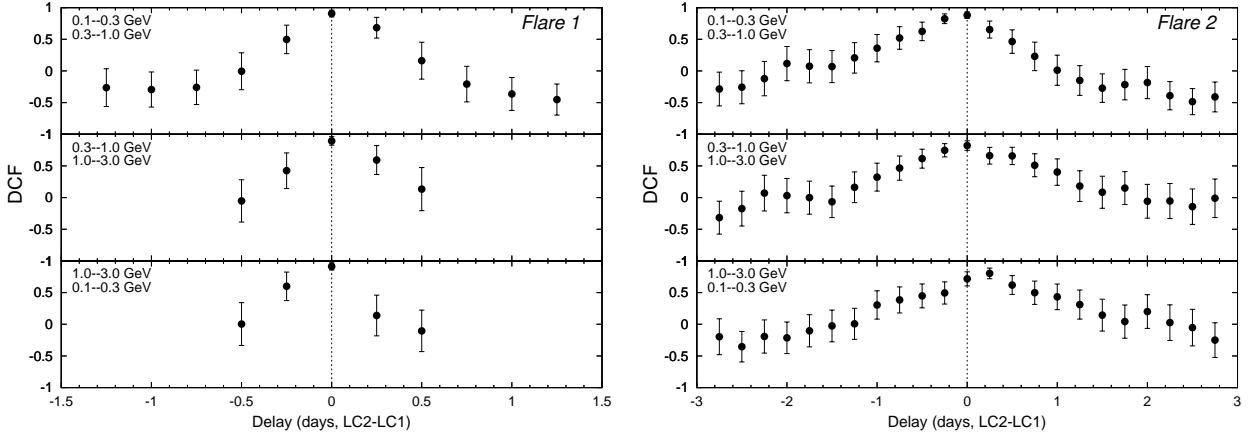


Fig. 4.— DCF calculated using uniformly sampled 6 hr light-curves for *Flare 1* (left) and *Flare 2* (right). The lag order used here is “LC2–LC1” light-curve as mentioned in each panel (see §3.3).

Table 3: Time lag\* values obtained for *Flare 1* and *Flare 2* using uniformly sampled 6 hr LAT data

LC1 Energy Band (GeV)	LC2 Energy Band (GeV)	<i>Flare 1</i> lag (days)	<i>Flare 2</i> lag (days)
0.1–0.3	0.3–1.0	$0.0^{+0.12}_{-0.11}$	$0.0^{+0.11}_{-0.19}$
0.3–1.0	1.0–3.0	$0.0^{+0.12}_{-0.11}$	$0.0^{+0.18}_{-0.21}$
1.0–3.0	0.1–0.3	$0.0^{+0.11}_{-0.12}$	$0.25^{+0.15}_{-0.20}$

\* T(LC2) – T(LC1) as given in columns 1 and 2

<sup>5</sup>lag study using non-uniformly sampled 6 hr data is also consistent with quoted results

#### 4. DISCUSSION

In this work, we have performed a detailed study of the two brightest  $\gamma$ -ray flares of PKS 1222+216 observed in *Fermi*-LAT in April and June 2010. The daily 0.1–300 GeV light-curve during these two flares has been systematically studied by dividing it into multiple energy bands (0.1–3, 0.1–0.3, 0.3–1 and 1–3 GeV) and using the shortest possible time binning (6 hr) allowed by the photon statistics. Contrary to a smooth rise followed by a rapid (*Flare 1*) or gradual (*Flare 2*) fall observed in the daily 0.1 – 300 GeV LAT  $\gamma$ -ray light-curves (top panel, Fig. 3), the 6 hr light-curves present a different case (Fig. 2). These 6 hr light-curves reveal a complex temporal behavior and variability patterns in different energy bands during the flaring episodes. *Flare 1* begins with a  $\sim 2$  day long plateau in the 0.1–0.3 GeV light-curve and enhanced variations at high energies with an apparent daily recurring pattern in 1–3 GeV light-curve. After this phase, a sharp increase in the flux is observed in all the LAT bands, followed by a rapid descent. To our knowledge, a plateau phase before flare has been a characteristic property of blazar 3C 454.3 (Abdo et al. 2011) but has not been seen in any other blazar during a flare. The absence of the plateau phase in the total energy integrated (0.1 – 300 GeV) daily light curve during *Flare 1*, suggests the rise may be governed primarily by  $> 0.3$  GeV photons (top panel, Fig. 3). In addition, presence of a plateau phase at lower energies is also reflected as the slow rise of daily binned 0.1-300 GeV  $\gamma$ -ray light curve during *Flare 1* (Figs. 1 & 3–top panel, §3). An exponential fit during the rising phase of the time and energy resolved light curves indicate a similar rise in all the bands except 0.3–1 GeV (Table 2, Fig. 2). If we consider a situation where a short lived acceleration mechanism (or a shock) is initiated in a turbulent jet, then the plateau phase may correspond to a case where the jet is becoming turbulent followed by the sudden rise probably due to a short lived acceleration. When the jet becomes turbulent, the electrons are accelerated via second order Fermi mechanism on a characteristic timescale,  $t_{\text{acc}}^{(t)} \sim (r_g/c)(c/V_A)^2$ , with acceleration rate  $\propto 1/t_{\text{acc}}$  (Rieger et al. 2007; Protheroe & Clay 2004; Bhattacharyya et al. 2005). Here,  $r_g$  is the electron gyro-radius and  $V_A$  is the Alfvén speed. On the other hand, shock acceleration is a first order Fermi mechanism with acceleration timescale  $t_{\text{acc}}^{(s)} \sim (r_g/c)(c/u_s)^2$ , where  $u_s$  is the speed of shock (Kirk & Dendy 2001; Protheroe & Clay 2004; Rieger et al. 2007). Hence, the turbulent acceleration rate lags the shock acceleration by a factor  $\sim (V_A/u_s)^2$  and the latter dominates the emission mechanism, once initiated.

In the case of *Flare 2*, the time and energy resolved light curves show a monotonic exponential rise from the beginning followed by a gradual descent with signatures of multiple peaks of decreasing strength from lower to higher energies (Fig. 2). The rate of rise of flux in all the energy bands are similar and also consistent with that of *Flare 1* (Table 2). The peak fluxes, during both the flares, are also similar in the respective energy bands except in the 1–3 GeV band during *Flare 1*, where the peak reaches approximately twice the corresponding peak flux during the *Flare 2*. This is, however, consistent with the observed “harder when brighter” trend seen during *Flare 1* (right panel, Fig. 1). Though the rate of rise are similar, the monotonic rise, lacking a plateau phase, probably causes the faster rise of the total energy integrated (0.1 – 300 GeV) daily-light curve compared to *Flare 1*. On the other hand, the slow decline of the daily, energy integrated 0.1–300 GeV light-curve is mainly due to the dominant contribution of 0.1–0.3 GeV emission with multiple peaks structures. This may be due to the contribution from multiple emission regions and their relative

locations (Nalewajko 2013; Giannios 2013) in addition to the standard flaring region contributing across the spectrum.

In contrast to the rising phase, the descent of the flux is faster in case of *Flare 1* but rather gradual in case of *Flare 2* (see Section §3). To further investigate the flare decay we obtained the physical parameters of the source by modeling the broadband SED using one zone leptonic model (Kushwaha et al. 2013; Sahayanathan & Godambe 2012). We used simultaneous/contemporaneous time averaged X-ray and LAT spectrum over the LAT flaring duration. The X-ray emission is reproduced considering SSC process whereas the  $\gamma$ -ray spectrum is reproduced considering external Compton scattering of the IR photons from a 1200 K dusty torus. The observed fluxes in X-rays and  $\gamma$ -rays during both the flares are similar and hence we assume that same set of physical parameters describe the source SED during the flares. The size of the emission region is constrained via the fastest observed rise time (0.4 day) while the particle indices are deduced from the X-ray and  $\gamma$ -ray spectra (Kushwaha et al. 2013). The final model spectrum along with the observed fluxes are shown in Fig. 5 and the corresponding parameters are given in Table 4. Based on these parameters, one can estimate the cooling timescale of the electrons emitting  $\gamma$ -rays in the observer’s frame as (Kushwaha et al. 2013, 2014; Saito et al. 2013)

$$\begin{aligned}
 t_{\text{cool}} &\simeq (3m_e c / 4\sigma_T U'_{\text{IR}}) \times \sqrt{(1+z)\epsilon_*/\epsilon_\gamma} \\
 &\sim 4 \left( \frac{\xi_{\text{ir}}}{0.15} \right)^{-1} \left( \frac{\Gamma}{22} \right)^{-2} \left( \frac{T_*}{1200\text{K}} \right)^{-7/2} \left( \frac{\epsilon_\gamma}{2\text{GeV}} \right)^{-1/2} \text{min}
 \end{aligned}
 \tag{1}$$

where  $\xi_{\text{ir}}$  ( $\sim L_{\text{IR}}/L_{\text{UV}}$ ) is the IR covering fraction with  $L_{\text{UV}}$  as the disk luminosity (Kushwaha et al. 2013),  $m_e$  is the rest mass of an electron,  $c$  is the speed of light and  $\sigma_T$  is the Thomson scattering cross-section. The IR photon energy density in the emission frame,  $U'_{\text{IR}}$  is related to the corresponding AGN frame energy density ( $U_{\text{IR}}$ ) as  $U'_{\text{IR}} = \Gamma^2 U_{\text{IR}}$ . The estimated cooling time scale (equation 1) is much smaller than the decay time of the flares obtained through the exponential fit of the light curves (Table 2) and hence we can conclude that decay of both the flares cannot be attributed to radiative cooling processes alone. If the decline is due to light travel time effects then one expects a similar decay times in all the energy bands, contrary to the one obtained (see Table 2). Alternatively, the flare decay can also be associated with the weakening of the acceleration process. In this case, one expects a steepening of spectral indices (Kirk et al. 1998). Both HR1 and HR2 during *Flare 1* show hardening during the rise followed by a softening to quiescent level (left panel, Fig. 3) during the decay. Relating this feature to the efficiency of particle acceleration process, we interpret the hardening of spectrum during rise as growth of shock acceleration process followed by its weakening, thereby softening the spectra during the flare decay. Contrary to the trend seen in *Flare 1*, the hardness ratios of *Flare 2* exhibit complex behavior. Here HR1 seems to harden till peak followed by a milder softening during decay whereas HR2 softens to its quiescent level at the peak and remains consistent with it throughout the decay (right panel, Fig. 3). Hence, unlike *Flare 1*, *Flare 2* cannot be interpreted as a result of single acceleration process but probably include other dynamical effects. The decay of *Flare 2* on daily timescales has been explained satisfactorily by considering the effects of jet dynamics. A decelerating jet interpretation can successfully reproduce the overall observed light-curves and SED (Kushwaha et al. 2014), though it seems that this model alone is not sufficient to explain the observed complex temporal behavior presented here. Nevertheless, this interpretation is supported by non-detection of significant lags

within various energy bands during the flare. The  $\sim 6$  hr lag observed in high energy during *Flare 2* can be a manifestation of different cooling processes (Dotson et al. 2012) and/or blob dynamics. Similar lags have also been found during the bright flares of FSRQ PKS 1510-089 (Brown 2013). However, the inferred lag is hard one contrary to soft lag found in our study. The absence of lag during *Flare 1* might be due to shorter duration of significant variation and averaging of data in the analysis of the same (see §3.2).

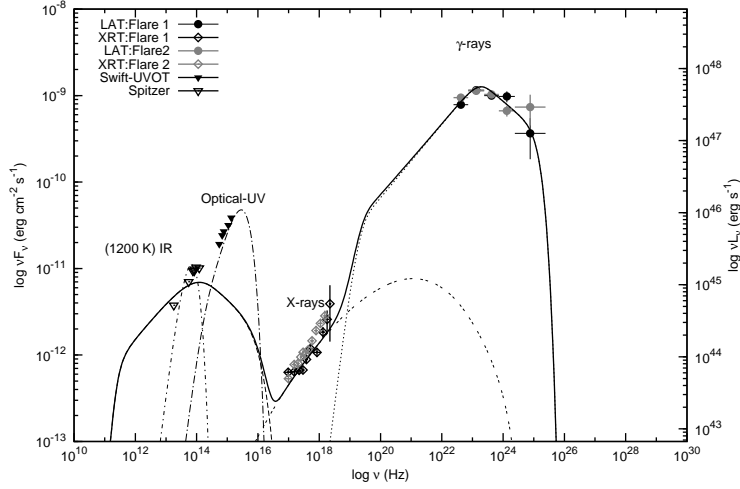


Fig. 5.— Broadband SED of PKS 1222+216 during *Flare 1* and *Flare 2* along with the model spectrum (§4).

Table 4: SED parameters for *Flare 1* and *Flare 2*

Parameters	Numerical values (CGS units)
Particle index before break ( $p$ )	2.15
Particle index after break ( $q$ )	3.6
Magnetic field ( $B$ )	0.35 G
Equipartition factor ( $\eta$ )	40
Doppler factor ( $\delta$ )	23
Angle to the line of sight ( $\theta$ )	$2.5^\circ$
Particle break energy* ( $\gamma'_{br}$ )	$2.3 \times 10^3$
Emission region size ( $R'$ )	$1 \times 10^{16}$
IR Torus temperature ( $T_*$ )	1200 K
Jet power ( $P_{jet}$ )	$2 \times 10^{46}$
Minimum particle energy* ( $\gamma'_{min}$ )	25
Maximum particle energy* ( $\gamma'_{max}$ )	$2 \times 10^4$

\*in electron rest-mass units

Based on lag and correlated-variability, both homogeneous and inhomogeneous model have been suggested for blazars' emission and have been successful in reproducing the observed SED and light-curves

of the sources (Tavecchio et al. 2011; Brown 2013; Kushwaha et al. 2013, 2014). Simple one-zone models have been found to satisfactorily reproduce the broadband SED during both the flares (Tavecchio et al. 2011; Ackermann et al. 2014; Kushwaha et al. 2014). However, the rise and fall within a day, during *Flare 1*, suggests that it probably arises from a  $\sim 0.5$  day long emission region as suggested by a similar rise time in all the LAT energy bands<sup>6</sup>. An indication of this daily variation is also apparent in the 1–3 GeV emission before rise. Moreover, contrary to this variation in 1–3 GeV emission, the 0.3–1 GeV emission suggests faster variation and has slowest rise and fall compared to the other two energy bands (Table 2). For *Flare 2*, various models including leptonic scenarios e.g. jet-in-jet/minijet (Tavecchio et al. 2011; Giannios 2013), recollimation (Aleksić et al. 2011; Tavecchio et al. 2011; Nalewajko et al. 2012; Kushwaha et al. 2014) and multiple emission zones (Tavecchio et al. 2011) along with hadronic scenario of ultra-relativistic neutral beams (Dermer et al. 2012) have been proposed. However, the temporal features seen in the systematic time and energy resolved study performed here demand scenarios beyond simple one zone homogeneous models where minor fluctuations are embedded within the region contributing to the major flare (H.E.S.S. Collaboration et al. 2012; Giannios 2013).

The two flares considered here have been studied earlier by Tanaka et al. (2011) and Nalewajko (2013). Both the previous studies focus on the spectral and temporal features in the 0.1–300 GeV energy band employing different time binning method. In this work, however, we have performed a more detailed and systematic time and energy resolved study. We have shown that all the features/patterns observed during *Flare 2* by Nalewajko (2013) are mainly due to features present at lower energies. Tanaka et al. (2011), on the other hand have termed these two flares as the highest possible  $\gamma$ -ray fluxes from PKS 1222+216, supposedly fueled by feeding the entire accretion power to the jet. However, the observed peak luminosity ( $L_{obs}$ ) which reaches  $\sim 10^{48}$  erg s<sup>-1</sup> during the peak corresponds to an emitted power of  $L_{em} \sim L_{obs}/2\Gamma^2 \simeq 1 \times 10^{45}$  erg s<sup>-1</sup> (Sikora et al. 1997) in the rest frame of the emission region, assuming a bulk Lorentz factor ( $\Gamma$ ) of 20 (Homan 2012; Ackermann et al. 2014). This is  $\sim 10\%$  of the accretion disk luminosity  $L_d \sim 3.5 \times 10^{46}$  erg s<sup>-1</sup> (Malmrose et al. 2011) and is in contrast to  $L_{em} \sim L_d$  derived by Tanaka et al. (2011), who assumed a comparatively lower value for the accretion disk luminosity  $L_d \simeq 5 \times 10^{45}$  erg s<sup>-1</sup> (assuming a BLR covering fraction  $\xi_{BLR} \simeq 0.1$ ) and jet bulk Lorentz factor  $\Gamma \simeq 10$ . A black hole of mass  $\sim 6 \times 10^8 M_\odot$  (Farina et al. 2012), however, can produce an Eddington luminosity of  $\sim 8 \times 10^{46}$  erg s<sup>-1</sup> which in turn suggests a very high accretion power and disk radiative efficiency. Apart from the asymmetry observed in the light-curves of the flares, Tanaka et al. (2011) found a hint of “harder-when-brighter” during *Flare 1* and a clockwise evolution in spectral index vs flux during *Flare 2*. Our analysis also reproduces these results but we found a clockwise trend during *Flare 1* as well, which is present in the study of Tanaka et al. (2011) but was probably suppressed due to the inclusion of a flare preceding the *Flare 1*.

---

<sup>6</sup>This is different from the  $\sim 10$  minutes variability considered by Ackermann et al. (2014) based on the VHE variability observed during *Flare 2*

## 5. CONCLUSIONS

We have performed an in-depth time and energy resolved study of the two brightest  $\gamma$ -ray flares from FSRQ PKS 1222+216 observed by the *Fermi*-LAT during April (*Flare 1*) and June (*Flare 2*) 2010. Our study reveals a large variety of temporal features and variability patterns in different energy bands (0.1–3, 0.1–0.3, 0.3–1.0 and 1–3 GeV) binned on 6 hr timescales apart from a clearly asymmetric profile in both the flares. This includes a  $\sim 2$  day plateau in 0.1–0.3 GeV band, hint of variation on daily timescale in 1–3 GeV emission, faster fluctuation ( $\sim 0.5$  days) at 0.3–1 GeV energy and a rapid decline during *Flare 1*. *Flare 2*, on the contrary, shows a monotonic rise followed by a gradual decline at all energies with prominent substructures in 0.1–0.3 GeV emission. Though the rise time are similar in all energy bands during both the flares, the slower rise of daily integrated 0.1–300 GeV light-curve during *Flare 1* is probably due to the presence of plateau in the 0.1–0.3 GeV emission with  $> 0.3$  GeV photons driving the initial rise. Further, the slower decline of 0.1–300 GeV light-curve during *Flare 2* is mainly due to contribution from the multiple peaked sub-structures in the 0.1–0.3 GeV light-curve resulting in a coherent single flare at daily timescales.

SED during both the flares can be well reproduced by a simple one zone model considering synchrotron, SSC and EC of IR emission mechanisms with similar parameters. The radiative cooling timescale of  $\sim 4$  min suggest that the observed duration and profiles of flares are not solely due to radiative cooling. The decline of flares also cannot be explained by considering light travel time effect which results in a similar decline rate at all energies, contrary to observations.

Study of hardness ratios during both the flares suggest that *Flare 1* can result from a variation in the efficiency of underlying acceleration process whereas for *Flare 2*, one need to consider the effect of jet dynamics and small scale inhomogeneities. The former contribute to overall flaring while the latter is responsible for the intrinsic feature observed in the time and energy resolved light-curves presented here. Based on these features we suggest that both flares are probably result of two different underlying mechanisms that are equally efficient in producing luminous  $\gamma$ -ray flares.

The *Fermi*-LAT Collaboration acknowledges generous ongoing support from a number of agencies and institutes that have supported both the development and the operation of the LAT as well as scientific data analysis. These include the National Aeronautics and Space Administration and the Department of Energy in the United States, the Commissariat à l’Energie Atomique and the Centre National de la Recherche Scientifique/Institut National de Physique Nucléaire et de Physique des Particules in France, the Agenzia Spaziale Italiana and the Istituto Nazionale di Fisica Nucleare in Italy, the Ministry of Education, Culture, Sports, Science and Technology (MEXT), High Energy Accelerator Research Organization (KEK) and Japan Aerospace Exploration Agency (JAXA) in Japan, and the K. A. Wallenberg Foundation, the Swedish Research Council and the Swedish National Space Board in Sweden.

Additional support for science analysis during the operations phase from the following agencies is also gratefully acknowledged: the Istituto Nazionale di Astrofisica in Italy and the Centre National d’Etudes Spatiales in France.

## REFERENCES

- Abdo, A. A., Ackermann, M., Ajello, M., et al. 2011, *ApJ*, 733, L26
- Ackermann, M., Ajello, M., Allafort, A., et al. 2014, *ApJ*, 786, 157
- Agudo, I., Marscher, A., Jorstad, S. G., & Gómez, J. L. 2013, *Highlights of Spanish Astrophysics VII*, 152
- Aleksić, J., Antonelli, L. A., Antoranz, P., et al. 2011, *ApJ*, 730, L8
- Alexander, T. 2013, arXiv:1302.1508
- Alexander, T. 1997, *Astronomical Time Series*, 218, 163
- Atwood, W. B., Abdo, A. A., Ackermann, M., et al. 2009, *ApJ*, 697, 1071
- Begelman, M. C., Fabian, A. C., & Rees, M. J. 2008, *MNRAS*, 384, L19
- Bhattacharyya, S., Sahayanathan, S., & Bhatt, N. 2005, *New A*, 11, 17
- Brown, A. M. 2013, *MNRAS*, 431, 824
- Bulgarelli, A., Gianotti, F., Trifoglio, M., et al. 2010, *The Astronomer's Telegram*, 2641, 1
- Carrasco, L., Carramiñana, A., Recillas, E., Porras, A., & Mayya, D. Y. 2010, *The Astronomer's Telegram*, 2626, 1
- Chiaberge, M., & Ghisellini, G. 1999, *MNRAS*, 306, 551
- Ciprini, S. 2009, *The Astronomer's Telegram*, 2349, 1
- Cooper, N. J., Lister, M. L., & Kochanzyk, M. D. 2007, *ApJS*, 171, 376
- Dermer, C. D., Murase, K., & Takami, H. 2012, *ApJ*, 755, 147
- Donato, D. 2010, *The Astronomer's Telegram*, 2584, 1
- Dotson, A., Georganopoulos, M., Kazanas, D., & Perlman, E. S. 2012, *ApJ*, 758, L15
- Farina, E. P., Decarli, R., Falomo, R., Treves, A., & Raiteri, C. M. 2012, *MNRAS*, 424, 393
- Finke, J. D., & Dermer, C. D. 2010, *ApJ*, 714, L303
- Fuhrmann, L., Larsson, S., Chiang, J., et al. 2014, *MNRAS*, 441, 1899
- Georganopoulos, M., Kirk, J. G., & Mastichiadis, A. 2001, *ApJ*, 561, 111
- Giannios, D. 2013, *MNRAS*, 431, 355
- H.E.S.S. Collaboration, Abramowski, A., Acero, F., et al. 2012, *A&A*, 539, A149



- Homan D. C., 2012, IJMPS, 8, 163
- Iafrate, G., Longo, F., & D’Ammando, F. 2010, The Astronomer’s Telegram, 2687, 1
- Kirk, J. G., Rieger, F. M., & Mastichiadis, A. 1998, A&A, 333, 452
- Kirk, J. G., & Dendy, R. O. 2001, Journal of Physics G Nuclear Physics, 27, 1589
- Kushwaha, P., Sahayanathan, S., & Singh, K. P. 2013, MNRAS, 433, 2380
- Kushwaha, P., Sahayanathan, S., Lekshmi, R., et al. 2014, MNRAS, 442, 131
- Kusunose, M., Takahara, F., & Li, H. 2000, ApJ, 536, 299
- Longo, F., Giroletti, M., & Iafrate, G. 2009, The Astronomer’s Telegram, 2021, 1
- MAGIC Collaboration, Albert, J., Aliu, E., et al. 2008, Science, 320, 1752
- Malmrose, M. P., Marscher, A. P., Jorstad, S. G., Nikutta, R., & Elitzur, M. 2011, ApJ, 732, 116
- Marscher, A. P. 2014, ApJ, 780, 87
- Mose Mariotti, M. 2010, The Astronomer’s Telegram, 2684, 1
- Mattox, J. R., Bertsch, D. L., Chiang, J., et al. 1996, ApJ, 461, 396
- Nalewajko, K. 2013, MNRAS, 430, 1324
- Nalewajko, K., Begelman, M. C., Cerutti, B., Uzdensky, D. A., & Sikora, M. 2012, MNRAS, 425, 2519
- Neronov, A., Semikoz, D., & Vovk, I. 2010, The Astronomer’s Telegram, 2617, 1
- Neronov, A., Semikoz, D., & Vovk, I. 2011, A&A, 529, A59
- Nolan, P. L., Abdo, A. A., Ackermann, M., et al. 2012, ApJS, 199, 31
- Poutanen, J., & Stern, B. 2010, ApJ, 717, L118
- Protheroe, R. J., & Clay, R. W. 2004, PASA, 21, 1
- Pushkarev, A. B., Kovalev, Y. Y., Lister, M. L., & Savolainen, T. 2009, A&A, 507, L33
- Rieger, F. M., Bosch-Ramon, V., & Duffy, P. 2007, Ap&SS, 309, 119
- Sahayanathan, S., & Godambe, S. 2012, MNRAS, 419, 1660
- Saikia, D. J., Wiita, P. J., & Muxlow, T. W. B. 1993, AJ, 105, 1658
- Saito, S., Stawarz, L., Tanaka, Y. T., et al. 2013, ApJ, 766, L11
- Sikora, M., Janiak, M., Nalewajko, K., Madejski, G. M., & Moderski, R. 2013, ApJ, 779, 68

- Sikora, M., Madejski, G., Moderski, R., & Poutanen, J. 1997, *ApJ*, 484, 108
- Striani, E., Verrecchia, F., Donnarumma, I., et al. 2010, *The Astronomer’s Telegram*, 2686, 1
- Tanaka, Y. T., Stawarz, Ł., Thompson, D. J., et al. 2011, *ApJ*, 733, 19
- Tavecchio, F., Becerra-Gonzalez, J., Ghisellini, G., et al. 2011, *A&A*, 534, A86
- Urry, C. M., & Padovani, P. 1995, *PASP*, 107, 803
- Vasileiou, V. 2013, *Astroparticle Physics*, 48, 61
- Verrecchia, F., Striani, E., Tavani, M., et al. 2009, *The Astronomer’s Telegram*, 2348, 1
- Wagner, S. J., & H.E.S.S. Collaboration 2010, *AAS/High Energy Astrophysics Division #11*, 11, #27.06